INSTITUTE OF PHYSICS PUBLISHING JOURNAL OF PHYSICS B: ATOMIC, MOLECULAR AND OPTICAL PHYSICS

J. Phys. B: At. Mol. Opt. Phys. **34** (2001) 965–981 www.iop.org/Journals/jb PII: S0953-4075(01)16502-8

Photo double ionization of He by circular and linear polarized single-photon absorption

M Achler[1], V Mergel[1], L Spielberger[1], R Dörner[2], Y Azuma[3] and H Schmidt-Böcking[1]

[1] Institut für Kernphysik, Universität Frankfurt, August Euler Straße 6, D60486 Frankfurt, Germany
[2] Fakultät für Physik, University Freiburg, Hermann Herder Straße 3, D79104 Freiburg, Germany
[3] Photon Factory, IMSS, KEK, Tsukuba, Ibaraki, 305 Japan

E-mail: rdoerner@uni-freiburg.de

Received 21 August 2000, in final form 27 November 2000

Abstract

We have measured absolute fully differential cross sections for photo double ionization of helium by circularly and linearly polarized light 20 eV above threshold. The data have been obtained by measuring in coincidence the momentum vector of the He^{2+} ion and one of the electrons, covering 4π solid angle for all particles. We give an overview over the momentum distribution in the three-body continuum and show fivefold differential cross sections. We find a swirl in the electron momentum space for double ionization by circularly polarized light. The present data supersede earlier data from our group (V mergel *et al* 1998 *Phys. Rev. Lett.* **80** 5301).

M This article features multimedia enhancements available from the abstract page in the online journal; see `www.iop.org`.

(Some figures in this article are in colour only in the electronic version; see `www.iop.org`)

1. Introduction

How does one photon couple to more than one electron? This question has been heavily studied over the past few years[4]. The first experimental and theoretical studies on two-electron ejection by photoabsorption considered only the total cross section for double ionization and the ratio of cross sections for double to single ionization [2–19]. Today, these questions are settled over the full energy range from threshold to 10 keV. Since the mid-1990s much more detailed experimental and theoretical studies have become available, initially discussing the energy sharing between the two emitted electrons [15, 20, 21], and finally dealing with coincident angular distributions of the two photo electrons (see [22] for a review) and the momenta and angular distributions of the recoiling He^{2+} ions [23–26]. Experimentally those studies have been performed by detecting both electrons in coincidence or by the cold-target

[4] A more detailed introduction to the different aspects of this problem can be found in [38].

0953-4075/01/060965+17$30.00

recoil-ion momentum spectroscopy (COLTRIMS [27]) technique. For linearly polarized light those studies cover the energy range from very close to threshold [28] to several tens of eV above the double-ionization limit. The high-energy regime is still completely unexplored.

For circularly polarized light dichroism, i.e. the dependence of the fully differential cross section on the helicity of the light in helium double ionization, has been predicted for the first time by Berakdar and Klar [29, 30]. They have shown that even if the initial state is spherically symmetric, circular dichroism (CD) is possible, whenever photon spin and the two electrons in the final state span a tripod with distinguishable legs. This was first confirmed experimentally by Viefhaus *et al* [31]. A much more complete coverage of the final-state phase space was achieved using the COLTRIMS technique in multibunch operation at the Photon Factory (Tsukuba) by us [1]. A large dichroism effect was found in the momentum space distributions of the recoiling He^{2+} ions for fixed direction of the fast electron. From these data the angular distribution of the photoelectrons has also been extracted. These electron angular distributions have recently been called into question by theoretical results [32, 33] and by a cross-check on consistency with well established results for linear polarization [34]. In addition recent experimental data on circular dichroism in He double photoionization by Soejima *et al* [35] found good agreement with CCC calculations by Kheifets and Bray in contrast to the conclusions drawn in [1]. The present paper resolves this dispute.

We have measured for an excess energy of 20 eV the fully differential cross section for linear and polarized light using the well established COLTRIMS technique in single-bunch operation of the photon factory. This experiment covers all angles and all energy sharings and also results in absolute cross sections.

2. Experiment

The experiment was performed at the Photon Factory, BL28A in single-bunch operation. The data reported here are taken over three consecutive days of beam time. We have switched the undulator from left circularly polarized (LCP) to right circularly polarized light (RCP) and linear polarization without altering our experimental set-up. Therefore, all possible systematical errors are the same in all data shown below. Note that LCP (optical definition) means that the polarization vector rotates counterclockwise for an observer looking towards the source. It is equivalent to right-hand or positive helicity (σ^+) in the quantum mechanical definition [36] and corresponds to photons with a magnetic quantum number $m = +1$, where m is the projection of the photon spin onto the direction of propagation. Also LCP corresponds to a negative value of the Stokes parameter S_3.

The experiment has been performed using the COLTRIMS technique (see [27, 37] for recent reviews). Details of the use of this technique for experiments on photo double ionization can be found in [38]. We have measured the momentum vector of one of the ejected electrons in coincidence with the charge state and momentum vector of the recoiling He^{2+} ion. The momentum vector of the second electron is calculated by exploiting momentum conservation.

The combined ion and electron spectrometer has 4π solid angle for the ions and for electrons up to 22 eV energy. Figure 1 shows a sketch of the experimental set-up. In brief the photon beam is intersected with a precooled supersonic He gas jet target. The gas jet had a width of about 1 mm at the intersection point. The ions were guided by a homogeneous electrostatic field (1.9 V cm^{-1}) followed by a drift region onto a position-sensitive channel plate detector with wedge-and-strip readout[5]. A set of Helmholtz coils (1.2 m diameter) generated a magnetic field of 11 G, parallel to the electric field. The combined electric and magnetic

[5] See Roentdek.com for details of the detectors.

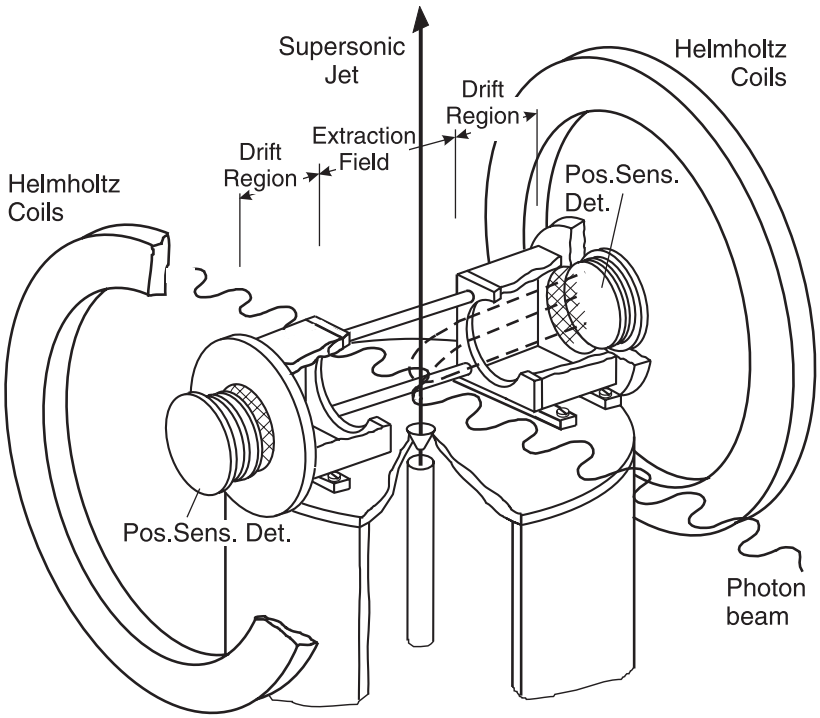

Figure 1. Recoil-ion momentum spectrometer as used in the present experiment. The supersonic gas jet is precooled. The electrons are accelerated to the left, the ions to the right. Both detectors are Z-stack channel plate detectors with an active area of 48 mm diameter and wedge-and-strip position readout. The Helmholtz coils are used to guide the electrons.

field guided the electrons onto a second position-sensitive detector (see [39] for a detailed description of the electron spectrometer). The fields yield 4π solid angle for electrons up to 22 eV energy. The combined electron detection efficiency of our channel plate and two grids is 30–40%. Those events where both electrons are detected are rejected based on the pulse height of the detector signal. For each electron and ion in every event, the position of impact and the time of flights with respect to the bunch marker of the storage ring was recorded in list mode.

The spectrometer was calibrated during the beam time using single ionization of He at photon energies of between 24 and 46 eV. For single ionization electron and ion momenta have equal magnitude, which is defined by the photon energy and the ionization potential. Due to momentum conservation these vectors have opposite direction (the photon momentum is negligible on this scale). This provides an ideal situation for the momentum calibration of the electron and the ion branch of the spectrometer. Furthermore, these calibrations provide enough information that the absolute value of the magnetic and the electric field can be obtained very accurately.

For double-ionization events, six momentum components can be obtained from the six measured quantities (positions of impact and the times of flight of the electron and ion). The three-body final state is characterized by nine momentum components of the three particles. Due to momentum and energy conservation only five of the nine momentum components are linearly independent. This provides redundancy in the experiment and allows for cross-checks against possible systematical errors (e.g. for each double-ionization event the sum energy of

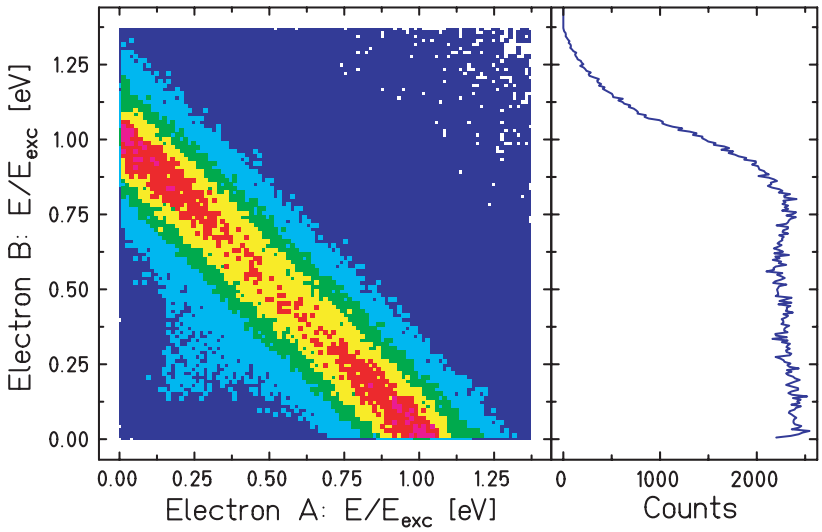

Figure 2. Distribution of energy between electrons A and B. The total excess energy is 20 eV. The right-hand side shows a projection, i.e. the energy distribution of electron B integrated over all angles of both electrons and all energy sharings.

both electrons can be obtained). Figure 2 shows the correlation between the energies of the two electrons. The width of the diagonal line shows the overall resolution of the system. The energy distribution of one of the electrons is shown in the right-hand panel. At 20 eV excess energy the energy distribution is almost flat, in agreement with earlier measurements [15, 20] and theoretical results [21]. The width of the high-energy edge again mainly reflects the resolution of the system, as explained in more detail below. Note that in experiments where two electrons are detected in coincidence by time-of-flight spectrometers [31, 40] the sum energy of both electrons has to be used to decide whether it was a random coincidence or a real double-ionization event. In our case, the charge state of the ion is detected and used to identify a double-ionization event. Therefore, the sum energy correlation shown in figure 2 is additional information which can be used for internal cross-checks in the momentum measurements.

The energy and angular resolution for the detected electron is determined mainly by the spatial extension of our gas jet. This uncertainty of the starting point of the electron trajectory in the joint electric and magnetic field translates in a highly nonlinear fashion into an uncertainty in the angle and energy determination. Thus the resolution varies widely as a function of energy and angle. An example is a resolution of $\Delta E = 0.05$ eV, $\Delta\Phi = 13^\circ$ at 2 eV for electrons starting in the direction of the electron detector. The worst case is, whenever the electron time of flight is an integer multiple of the cyclotron frequency. At these points in electron phase space the error diverges. They are a very small fraction of the total final-state phase space and are excluded in our analysis (see [39] for a more detailed discussion of this type of electron imaging spectrometer). For the recoil-ion momentum measurement our spectrometer has a fixed absolute momentum uncertainty in all three dimensions which is 0.14 au FWHM in the direction of the electric field and about 0.29 au FWHM in the direction of the gas jet and the photon beam. The width of the diagonal (about 5.5 eV) in figure 2 reflects the sum of all of these errors and nonlinearities. The contribution of the photon bandwidth (about 1 eV) to this sum energy is almost negligible.

Since the experiment covers the full phase space of the final state (4π solid angle for electron and ion) the absolute normalization is straightforward. The total number of valid counts corresponds to the total cross section.

The experimental procedure used here is superior to that used in our earlier work [1] in three important aspects.

(a) No magnetic field for the electron confinement has been used in [1].
(b) A retarding voltage directly in front of the channel plate was used in [1] to repel electrons with energy below 11 eV.
(c) The most important difference was the lack of a beam bunchclock in [1], as the previous experiment was performed during multibunch operation of the storage ring.

(a) and (b) together resulted in a solid angle of well below 1π for the detected electron. More importantly, as a consequence of (c) for each event the positions of impact and the flight time *difference* between the electron and ion were measured, not the individual times of flight. From these five quantities all nine momentum components could be obtained using momentum and energy conservation. In addition to the conservation rules, the detected electron must be known to be the fast electron (by a retarding field (b)) to eliminate the ambiguity of a sign in solving a quadratic equation. However, there was no redundancy in calculating the momenta, which allowed for cross-checks against possible systematical errors. For example, the exact value for the fields in the spectrometer and for the absolute photon energy entered crucially in the analysis. In particular, the absolute value of the time difference between the electron and ion was critical.

The use of single-bunch mode and thus a bunch marker signal in the present experiment eliminates all of these potential problems. Since here the time-of-flight for the electron and ion are known, the calculation of momenta of both particles is decoupled and straightforward. This technique has been used with great success in many experiments for ion and photon impact [27]. Furthermore, the determination of the absolute value of the cross section was subject to bigger potential errors in the previous experiment, since the spectrometer did not cover 4π for the electrons. Therefore, the fraction of the solid angle which was covered had to be calculated and the energy distribution of the electrons had to be extrapolated. This introduced a much bigger systematic error on the absolute normalization compared with the present experiment.

The primary data in the previous as well as in the present experiment are the momentum distributions of the recoiling He^{2+} ions for fixed momentum vector of one of the electrons. These recoil-ion momentum distributions show a strong effect of circular dichroism (see figure 2 in [1]). Figure 3 shows the recoil-ion momentum distribution in the plane perpendicular to the photon beam from the present experiment. The recoil ion and electron (indicated by the arrow) are both confined to this plane perpendicular to the photon propagation. The left-hand panel shows the ion momenta with no restriction of the electron energy. The distribution is highly asymmetric to the horizontal, showing the large effect of the circular dichroism. For comparison with our previous results (see figure 2 in [1]) the right-hand panel shows our present data with a restriction to electron energies greater than 11 eV, to simulate the retarding grid used in the previous experiment. We find a much higher resolution but the general features observed in both experiments are identical. In the previous experiment the momentum vector of the measured electron (horizontal axis in figure 1 in [1] and figure 3 of this paper) is obtained predominantly from the time-of-flight difference between the recoil ion and electron. A potential problem in the determination of the time zero position in the time-of-flight spectrum results in a shift of the origin in figure 3. From these data electron angular distributions and 5DCS are generated. A possible shift of the origin in figure 3 does not change the observed ion momentum pattern, but mainly changes the opening angle of the two lobes of the 5DCS

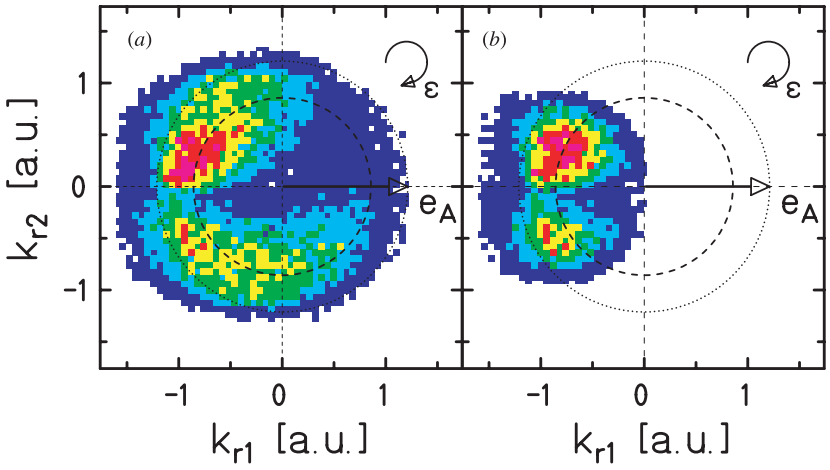

Figure 3. Momentum distribution of the recoiling He^{2+} ion for RCP. One electron is fixed to the right (arrow). The plane shown is perpendicular to the propagation of the light. Only those events are plotted where the electron and ion are emitted in this plane ($\theta_{\rm ion} = \theta_{\rm A} = 90 \pm 20^{\circ}$). Electron A has no fixed direction in the laboratory frame (see the discussion in section 3). Left, no restriction on the electron energy; right, electron energy >11 eV (this is to be compared with figure 2 in [1]).

and influences the absolute calibration. We have propagated the errors by analysing our data with different assumptions on the zero points. One example is shown in figure 4, where the zero point of the ion momentum has been shifted by ± 0.05 au (see [41] for more examples). As we will see below this is not sufficient to explain the discrepancy between our old and new experiments, showing that our estimate of systematical errors in [1, 41] was too optimistic. In the present experiment such potential problems are avoided since the time of flight of the ion and electron are measured independently with respect to the beam clock. A comparison of the present and previous results for the electron angular distribution is discussed below.

3. Influence of the Stokes parameters

As discussed above, the double-ionization process is fully characterized by five linearly independent quantities. One could choose for example five momentum components or alternatively the energy sharing and the polar ($\theta_{\rm A}, \theta_{\rm B}$) and azimuthal ($\phi_{\rm A}, \phi_{\rm B}$) angle of each of the two electrons A and B with respect to any axis. The polar and azimuthal angle are often noted jointly as a (two-dimensional) solid angle $\Omega_{\rm A}, \Omega_{\rm B}$. Double photo ionization can hence be fully described by a fivefold differential cross section (5DCS). The measured 5DCS depends on the polarization characteristics of the light as given by the Stokes parameters S_1 and S_3. The measured $5{\rm DCS}^{\rm exp}$ is an incoherent sum of the cross section for LCP and RCP light $5{\rm DCS}^{\rm LCP,RCP}$ and for linearly polarized light $5{\rm DCS}^{{\rm lin}_{x,y}}$ along two axes x and y, which are perpendicular to each other and perpendicular to the propagation of the light (see [42]):

$$5{\rm DCS}^{\rm exp} = \tfrac{1}{2}(5{\rm DCS}^{{\rm lin}_x} + 5{\rm DCS}^{{\rm lin}_y}) + \tfrac{1}{2}S_1(5{\rm DCS}^{{\rm lin}_x} - 5{\rm DCS}^{{\rm lin}_y}) + \tfrac{1}{2}S_3(5{\rm DCS}^{\rm RCP} - 5{\rm DCS}^{\rm LCP}). \quad (1)$$

Throughout this paper we choose the laboratory frame where x is parallel to the plane of the storage ring (parallel to the electric extraction field in figure 1 and y is perpendicular to the ring (along the direction of the gas jet in figure 1).

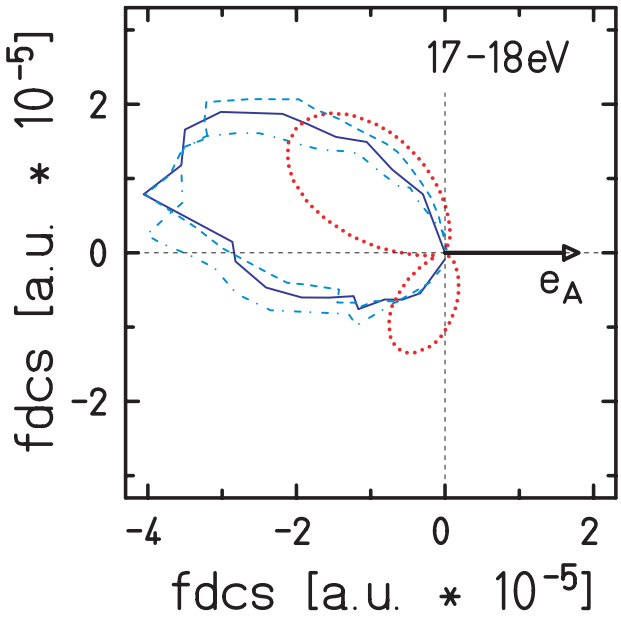

Figure 4. Analysis of systematical errors of our earlier experiment from [1]. 5DCS for $E_\gamma = 99$ eV, LCP, electron A is emitted with 13.5 eV in the direction of the arrow. Both electrons are confined to the plane perpendicular to the light propagation. The full curve shows the results using the analysis as in [1], the long- and short-broken curves show the same raw data resorted with the zero point of the recoil-ion momentum shifted by ± 0.05 au. The dotted curve shows the CCC-calculation of Kheifets and Bray.

For beamline BL28A of the photon factory Kimura *et al* [43] measured for the standard setting at 97 eV for RCP and LCP $S_1 = -0.2$, $S_3 = +0.95$ in a frame tilted by 134° with respect to the plane of the storage ring and $S_1 = 0.2$, $S_3 = -0.95$ in a frame tilted by 44°. We did not determine the Stokes parameters in the present experiment. In our previous experiment we found $S_1 = 0.29 \pm 0.03$ from the angular distribution of the electron from single ionization. Assuming that the degree of polarization $P = \sqrt{S_1^2 + S_3^2}$ was not smaller than $P = 0.97 \pm 0.1$ [43] we obtain $S_3 = 0.93 \pm 0.01$ in [1]. We confirm the tilt of the main axis of the polarization ellipse as one switches the beamline from the LCP to the RCP mode of the beamline.

As a consequence of the 4π solid angle for the ion and electron realized in the present experiment, we can use symmetries in the laboratory frame to make our final data completely insensitive to the main axis of the linearly polarized contribution of the light, as we will show now. For circularly polarized light the beam axis is the symmetry axis of the process. Therefore, we use polar coordinates where θ_A and θ_B denote the polar angles of electrons A and B with respect to the beam axis and ϕ_A and ϕ_B are the azimuthal angles around the beam axis, with $\phi = 0$ being parallel to the plane of the storage ring. $5\mathrm{DCS}^{\mathrm{RCP,LCP}}$ does not depend on ϕ_A and ϕ_B individually but only on the relative azimuthal angle $\phi_{AB} = \phi_A - \phi_B$. We switch in our data analysis from the angle pair (ϕ_A, ϕ_B) to the pair (ϕ_A, ϕ_{AB}) and then integrate the data over ϕ_A. Thus we sample all events with fixed ϕ_{AB} while summing over the laboratory azimuthal angles ϕ_A and ϕ_B. This allows one to gather the statistics from all physically equivalent configurations of electron phase space. Using equation (1) the experimental fourfold differential cross section

obtained by this procedure is given by

$$4\mathrm{DCS}^{\mathrm{exp}}(\phi_{\mathrm{AB}}, \theta_{\mathrm{A}}, \theta_{\mathrm{B}}, E_{\mathrm{A}}) = \frac{1}{2\pi}\Bigg(\int_{\phi_{\mathrm{A}}=0}^{\phi_{\mathrm{A}}=2\pi} \tfrac{1}{2}(5\mathrm{DCS}^{\mathrm{lin}_x} + 5\mathrm{DCS}^{\mathrm{lin}_y})\,\mathrm{d}\phi_{\mathrm{A}} + \int_{\phi_{\mathrm{A}}=0}^{\phi_{\mathrm{A}}=2\pi} \tfrac{1}{2}S_1(5\mathrm{DCS}^{\mathrm{lin}_x} - 5\mathrm{DCS}^{\mathrm{lin}_y})\,\mathrm{d}\phi_{\mathrm{A}} + \int_{\phi_{\mathrm{A}}=0}^{\phi_{\mathrm{A}}=2\pi} \tfrac{1}{2}S_3(5\mathrm{DCS}^{\mathrm{RCP}} - 5\mathrm{DCS}^{\mathrm{LCP}})\,\mathrm{d}\phi_{\mathrm{A}}\Bigg). \tag{2}$$

For a beta parameter $\beta = 0$ of the electron, which is reasonably fulfilled at 20 eV excess energy [23, 24], the second integral is identically zero. Berakdar [44] has shown (see also figure 10 and the related discussion below) that the first integral can be expressed by 5DCS for circularly polarized light:

$$\int_{\phi_{\mathrm{A}}=0}^{\phi_{\mathrm{A}}=2\pi} (5\mathrm{DCS}^{\mathrm{lin}_x} + 5\mathrm{DCS}^{\mathrm{lin}_y})\,\mathrm{d}\phi_{\mathrm{A}} = \int_{\phi_{\mathrm{A}}=0}^{\phi_{\mathrm{A}}=2\pi} (5\mathrm{DCS}^{\mathrm{RCP}} + 5\mathrm{DCS}^{\mathrm{LCP}})\,\mathrm{d}\phi_{\mathrm{A}}. \tag{3}$$

Thus equation (2) simplifies to

$$4\mathrm{DCS}^{\mathrm{exp}}(\phi_{\mathrm{AB}}, \theta_{\mathrm{A}}, \theta_{\mathrm{B}}, E_{\mathrm{A}}) = \frac{1}{4\pi}\int_0^{2\pi} (1 + S_3)5\mathrm{DCS}^{\mathrm{RCP}} + (1 - S_3)5\mathrm{DCS}^{\mathrm{LCP}}\,\mathrm{d}\phi_{\mathrm{A}}. \tag{4}$$

Note that as a consequence of the integration the 5DCS for linearly polarized light no longer enters directly into the observed 4DCS, no matter what the Stokes parameter of the light is. Therefore, the direction of the main polarization axis and the linear dichroism [35] also no longer affects the data. The only remaining influence of $S_3 < 1$ is that it reduces the contrast of the circular dichroism. This is in contrast to the situation in experiments where one electron spectrometer is fixed in the laboratory frame and the second one is rotated [35].

We performed two experiments while switching the undulator from the RCD to the LCP mode, yielding $4\mathrm{DCS}^{\mathrm{exp}}_{\mathrm{RCP}}$ and $4\mathrm{DCS}^{\mathrm{exp}}_{\mathrm{LCP}}$. From these raw data we can calculate the cross section for purely circularly polarized light:

$$4\mathrm{DCS}^{\mathrm{RCP}}(\phi_{\mathrm{AB}}, \theta_{\mathrm{A}}, \theta_{\mathrm{B}}, E_{\mathrm{A}}) = \frac{1}{2}\left(\left(1 + \frac{1}{S_3}\right)4\mathrm{DCS}^{\mathrm{exp}}_{\mathrm{RCP}} + \left(1 - \frac{1}{S_3}\right)4\mathrm{DCS}^{\mathrm{exp}}_{\mathrm{LCP}}\right). \tag{5}$$

Since $S_3 = 0.95$ this is a very small correction to the raw data (see figure 6(*a*)).

4. Correlated electron momentum space distributions

In this section we show the main results of this work. A complete overview of the structure of the three-body continuum after absorption of a linear and a circularly polarized photon is given in figure 5. This presentation makes use of the main advantage of the COLTRIMS technique to cover the full solid angle and all energy sharings at once. No preselection of angles and energies has to be made in the experiment.

Due to momentum conservation, the momentum vectors of both electrons and the ion are always in one plane (neglecting the photon momentum). This internal plane of the three-body breakup is shown in all panels of figure 5. The direction of one of the electrons (labelled electron A) is shown by the arrow, and the momentum distribution of the second electron (B) is given by the density distribution. Since the sum energy of the electrons is fixed by the photon energy, the magnitude of the momenta (i.e. the radius drawn around the origin) is coupled. The outer circle indicates the locus of events where electron B has all the excess energy, the inner

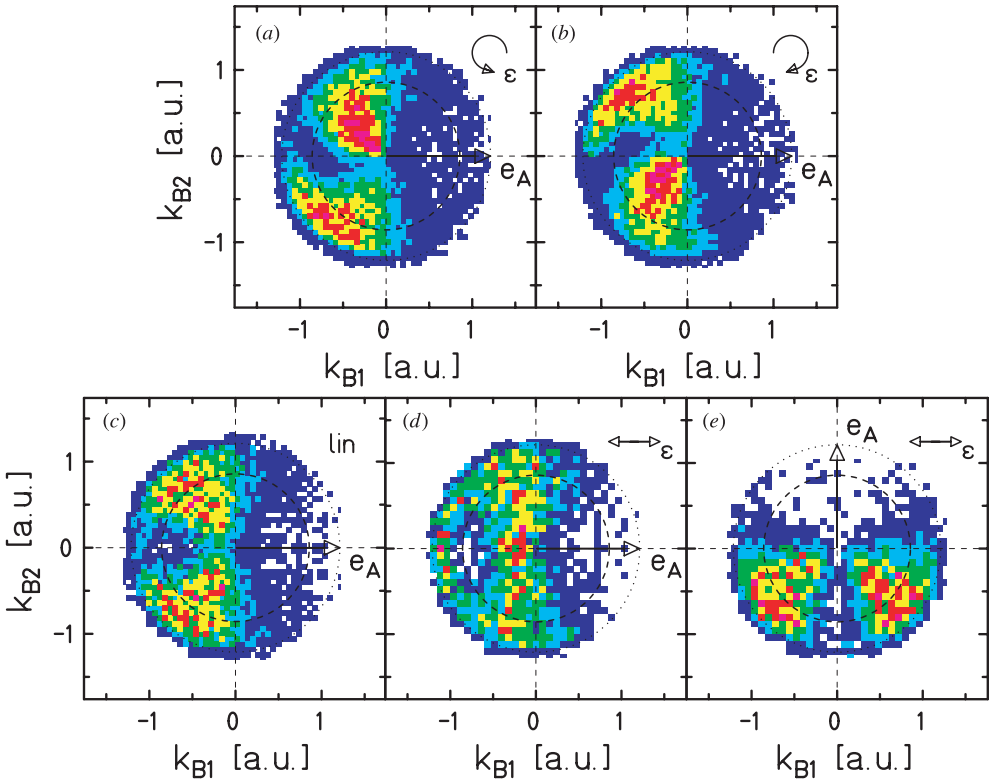

Figure 5. Momentum distribution of electron B with respect to electron A. The arrow indicates the direction of electron A. The outer circle is the maximum possible momentum, the inner circle indicates the locus of events with equal energy sharing (20 eV excess energy). (*a*) and (*b*) are for LCP and RCP, respectively. The plane shown in (*a*) and (*b*) is perpendicular to the propagation of the light ($\theta_A = \theta_B = 90 \pm 20^\circ$). Only those events are plotted where both electrons are emitted in this plane. Electron A has no fixed direction in the laboratory frame (see the discussion in section 3). (*c*) Linearly polarized light. The figure is integrated over all orientations of the polarization axis, thus the plane shown has no fixed orientation in the laboratory. (*d*) and (*e*) show subsamples of the all events displayed in (*c*) with electron A parallel (*d*) and perpendicular (*e*) to the polarization ϵ, which is horizontal.

circle indicates the case of equal sharing of the excess energy among the electrons. Figures 5(*a*) and (*b*) show results for circular and (*c*)–(*e*) results for linearly polarized light. The data in figure 5(*c*) are integrated over all directions with respect to the polarization, i.e. the sum over all events displayed gives the total double-ionization cross section. Figures 5(*d*) and (*e*) show only the subset of events where the momentum of electron A is parallel or perpendicular to the polarization axis (which is horizontal in both panels). In figures 5(*a*) and (*b*) the circularly polarized photons propagate into the plane of the paper, and both electrons are restricted to a polar angle of $90^\circ \pm 20^\circ$ with respect to the photon propagation, i.e. only a subspace of the final state is shown.

Two well known features of the breakup process are visible in all panels. First, both electrons emerge predominantly in opposite half-spheres (due to electron repulsion). Second, there is a node in the correlated wavefunction for equal energy sharing and back-to-back emission. This node is a result of the $^1P^o$ symmetry of the final state for double ionization of He by absorption of one photon [45]. Both effects have been seen already in the first

pioneering experiment by Schwarzkopf *et al* [46]. Both features prevail for linearly polarized light, independently of the directions of the first and second electrons to the polarization (figures 5(*c*)–(*e*)) and left and right circularly polarized light (figures 5(*a*) and (*b*)). The $^1P^o$ symmetry implies a node at the point $k_1 = -k_2$, and the experiment shows that this node is not an isolated feature but a well extended area in momentum space. Only for very unequal energy sharing (see also [47, 48]) is an appreciable count rate found for antiparallel emission of the electrons. For the subspace of one electron being emitted perpendicular to the polarization (figure 5(*e*)) the nodal area around $k_1 = -k_2$ extends to a nodal line for antiparallel emission for all energy sharings (see [45, 49] selection rule F, and [38]).

The data for circularly polarized light show that the node for antiparallel emission at equal energy sharing is part of a curved line of reduced momentum space density (figures 5(*a*) and (*b*)). This swirl in momentum space is not a result of a symmetry-based selection rule but a non-trivial consequence of the detailed dynamics of the process. It is a visual consequence of the rotation of the electric field vector of the circularly polarized light which puts a torque into the electron pair motion [50]. This is possibly related to a rotation of the forward peak in photoelectron diffraction [52–55]. We will discuss this in some more detail in the conclusions.

5. Fivefold differential cross section

Figures 5(*a*) and (*b*) shows the complete information on the double-ionization process. It is not integrated over any coordinate, since the plane is fixed perpendicular to the direction of the light. To allow for an easier comparison with other data and with theory we display parts of the same data in the more traditional representation of differential cross sections in polar and azimuthal angle and energy of the electrons.

Figure 6 shows the fourfold differential cross section $\mathrm{d}^4\sigma/\mathrm{d}\phi_{\mathrm{A,B}}\,\mathrm{d}\cos(\theta_{\mathrm{A}})\,\mathrm{d}\cos(\theta_{\mathrm{B}})\,\mathrm{d}E_{\mathrm{A}}$ for double ionization of helium by circularly polarized light. θ_{A}, θ_{B} denote the polar angles of electrons A and B with respect to the direction of propagation, and ϕ_{AB} is the corresponding azimuthal angle between the two electrons. As in figure 5 we restrict ourselves to emission of both electrons in the plane perpendicular to the direction of propagation of the light ($\theta_{\mathrm{A}} = \theta_{\mathrm{B}} = 90^\circ \pm 10^\circ$). All panels show a polar plot of the angle ϕ_{AB}. The direction of one of the electrons is indicated by the arrow. We have chosen four different sharings of the excess energy. Figures 6(*a*)–(*d*) show a comparison of our data for left- and right-hand circularly polarized light. For equal energy sharing, no significant difference between the two experiments, and thus no dichroism, is observed. This is a consequence of the indistinguishability of the two electrons with equal energy. The comparison of both polarizations serves as a test of systematical errors in the experiment. In the middle and left row we have added our data for LCP and RCP. In figure 6(*a*) the raw data, not corrected according to equation (5), are shown together with the calculated FDCS for $S_3 = 1$. All other panels as well as all the following figures show only the calculated final results for pure circular polarization.

The dichroism also does not vanish for extremely unequal energy sharing (figure 6(*a*)). A necessary condition for the appearance of circular dichroism in double photoionization of helium is that the two electron momentum vectors and the light propagation axis span a tripod with a defined handedness. For equal energy sharing two legs of this tripod are indistinguishable, thus no dichroism is possible. For extreme unequal energy sharing the length of one of the legs goes to zero. The remaining dichroism shows that the pure existence of two distinguishable electron momentum vectors is sufficient for dichroism to appear and that it does not go to zero as the magnitude of one of the momenta diminishes. Note that the data shown in figures 6 are a small subsample of the final phase space and of the recorded

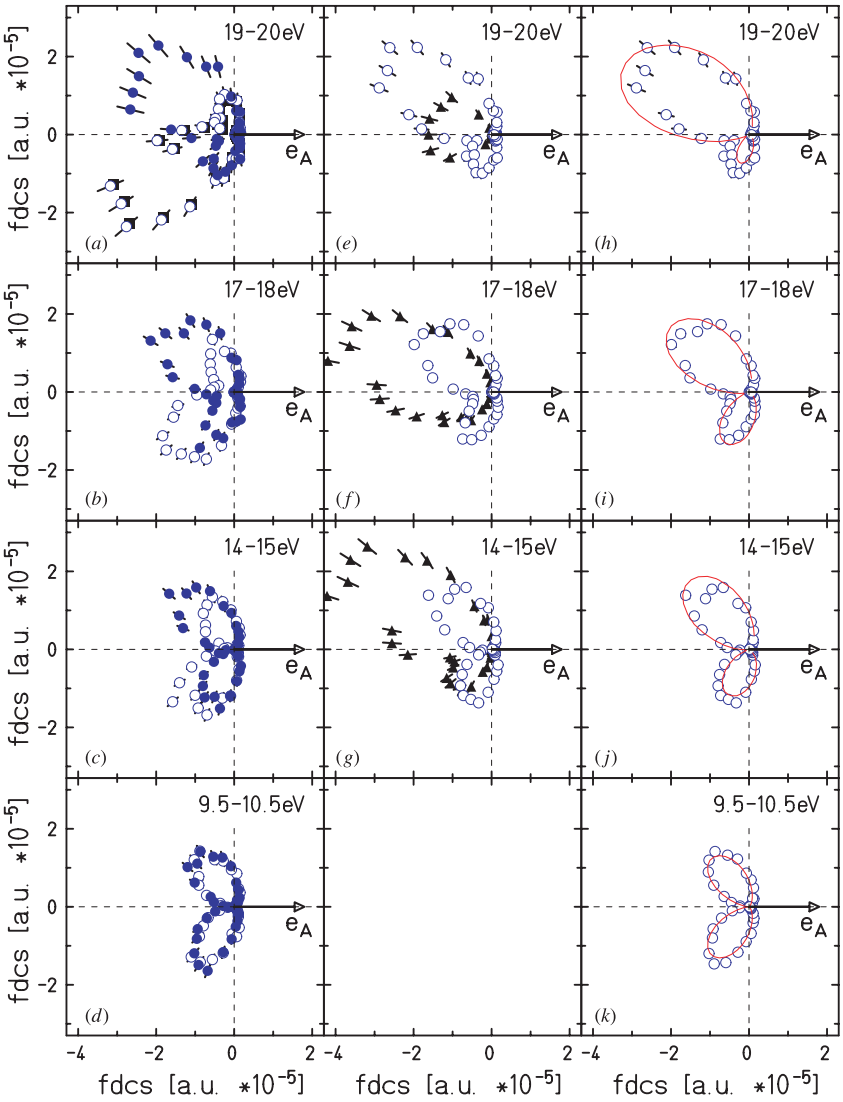

Figure 6. Fourfold differential cross section $d^4\sigma/d\phi_{AB}\, d\cos(\theta_A)\, d\cos(\theta_B)\, dE_A$ for circularly polarized light. The azimuthal angle ϕ_{AB} around the photon axis between electrons A and B is plotted. The polar angles to the photon propagation are $\theta_A = \theta_B = 90^\circ \pm 10^\circ$. The energy sharing is indicated in the figure. Electron A has no fixed direction in the laboratory frame (see the discussion in section 3). Left column, comparison of data for LCP (full triangles) and RCP (open triangles), the full symbols overlapping with the open triangles in (*a*) show our raw data, all other symbols in this and the following figures show results for pure circularly polarized light calculated from the raw data using equation (5); middle column, comparison of present data (open circles) with data from our previous experiment in multibunch mode from [1] (full symbols) (see the discussion in the text); right column, full line in the upper three panels, CCC calculations from [32]; full line lower panel, parametrization. All data are on an absolute scale, the middle and left columns show the accumulated data from LCP and RCP. A smooth evolution of the angular distribution as a function of energy sharing can be found in the animated gif in the online version of this paper. The movie shows data with $\theta_A = \theta_B = 90^\circ \pm 10^\circ$, the energy of electron A has been integrated over a range indicated in the movie.

M An animated GIF of this figure is available from the article's abstract page in the online journal; see www.iop.org.

data. The transition of the angular distributions as a function of the energy sharing is shown in more completeness in the movie (animated gif) which can be found in the online version of this paper.

The middle column of figures 6(*e*)–(*g*) show a comparison of the present data with 4DCS from our previous experiment from [1] which was taken under the much inferior experimental conditions of multibunch operation as explained in the experimental section above. There is a clear discrepancy between the data in the absolute value as well as in the opening angle of the two lobes. Possible sources for this in the previous experiment are discussed above. Comparison with figure 4 shows that our new, correct, data are outside the estimated systematic error of our earlier, inferior, experiment. It is not clear to us which of the possible sources of systematic error we had underestimated. In addition to the redundancy checks in the momentum measurement we point out that the reliability of our present experiment is supported by the smooth disappearance of the dichroism at equal energy sharing. In our previous experiment equal energy sharing was not detected due to the retarding grid in front of the electron detector. Furthermore, in the present case we detect each energy sharing twice. The detected electron can be either the fast electron or the slow electron. The momentum of the remaining electron is then obtained via the recoil ion. These two cases, where the fast or the slow electron is detected, show identical results within the given error bars.

Figures 6(*h*)–(*j*) show a comparison of our present data with convergent close-coupling calculations by Kheifets and Bray [32]. The agreement on absolute scale is excellent. The major disagreement between CCC and the experimental data on circular polarization reported in [32] were, as the authors suggest, caused by experimental problems in our previous work [1]. For our present data CCC gives a slightly incorrect ratio between the two lobes at the most unequal energy sharing. Similarly Cvejanovic *et al* [55] have reported the highest discrepancy with CCC for double ionization for extremely unequal energy sharing by linear polarized light. In addition, figure 6(*k*) shows a comparison of the present data with a fit with a Gaussian correlation function (FWHM $= 91^\circ$).

The normalized difference between the countrates for LCP and RCP has been termed circular dichroism (see, e.g., [1, 29, 31, 56]):

$$\mathrm{CD}(\phi_{\mathrm{AB}}, \theta_{\mathrm{A}}, \theta_{\mathrm{B}}, E_{\mathrm{A}}) = \frac{4\mathrm{DCS}^{\mathrm{LCP}} - 4\mathrm{DCS}^{\mathrm{RCP}}}{4\mathrm{DCS}^{\mathrm{LCP}} + 4\mathrm{DCS}^{\mathrm{RCP}}}. \tag{6}$$

The CD obtained from the data from figures 6(*a*)–(*d*) is shown in figure 7 together with our previous results from [1] and the CCC and 3C calculation. Note that in some respects the CD is less sensitive to systematical experimental errors than the 4DCS, since errors (in particular, in the absolute height) tend to cancel each other in the CD. This is clearly seen by comparison of our old and present experimental data in figures 6 and 7 as well as in the comparison with theory. Figure 8 shows the CD as a function of the energy of electron A at a fixed angle, highlighting the change of sign of the CD at equal energy sharing.

Part of our data for linear polarization are shown in figure 9 for three different energy sharings. Again good agreement is found with CCC calculations. The data are also in good agreement with experimental results of Bräuning *et al* [57]. For equal energy sharing again the angular distributions are well described by a Gaussian correlation function. The present data on linearly polarized light are measured in the same beam time as the above data for circularly polarized light, by only changing the undulator and not the COLTRIMS set-up. Thus, the good agreement of the present data shown in figure 9 with earlier, completely independent experiments and theory, is a further cross-check on our present experiment.

Berakdar has pointed out that the cross sections obtained with linearly and circularly polarized light can be compared directly [44]. He showed that the sum of the differential cross

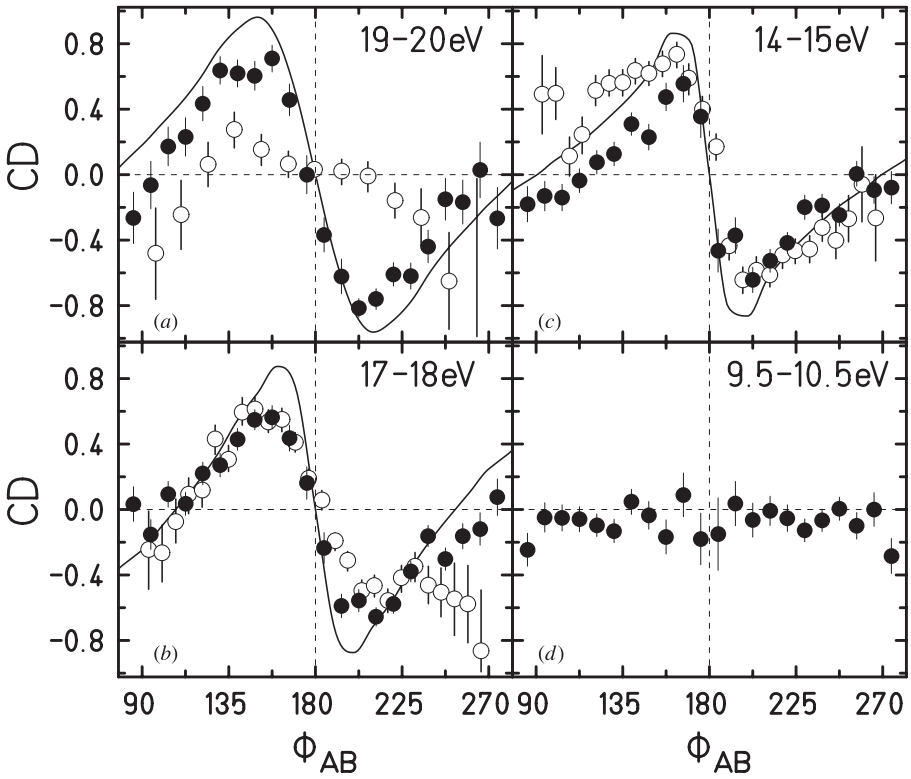

Figure 7. Circular dichroism as defined in the text. Geometry a in figures 5(*a*)–(*d*). Full symbols, present work; open symbols, data from our previous experiment in multibunch mode from [1]. Full curve, CCC calculations from [32].

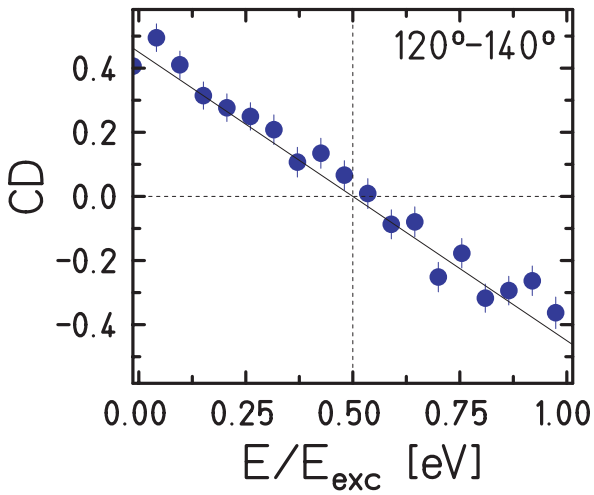

Figure 8. Circular dichroism (CD, see text for definition) as a function of energy sharing. $\theta_A = \theta_B = 90 \pm 10^\circ$ (as in figures 5 and 6), $\phi_{AB} = 130 \pm 10^\circ$.

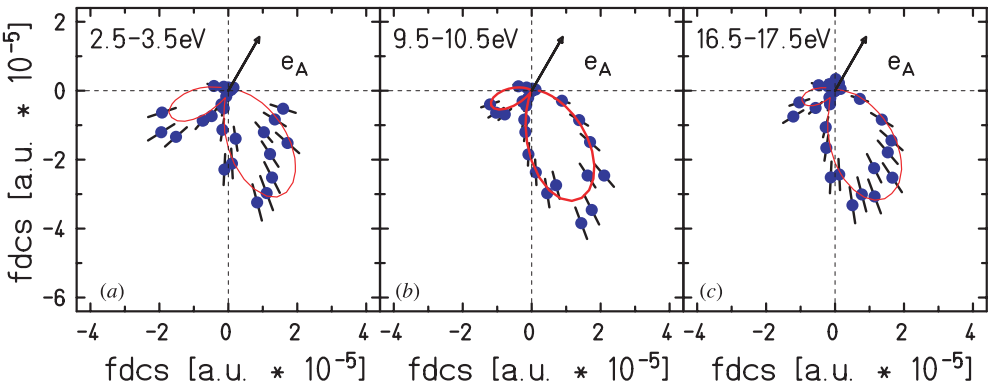

Figure 9. Fourfold differential cross section $d^4\sigma/d\phi_{AB}\, d\cos(\theta_A)\, d\cos(\theta_B)\, dE_A$ for linearly polarized light. Symbols, polar angular distribution of electron B with respect to the polarization which is horizontal. Polar angle $\theta_A = 50°$–$70°$, azimuthal angle $\Phi_A = 0° \pm 20°$, $\Phi_B = 0° \pm 20°$. Full curve, left and right panels, CCC calculations from [32]; middle panel, parametrization with a Gaussian correlation function.

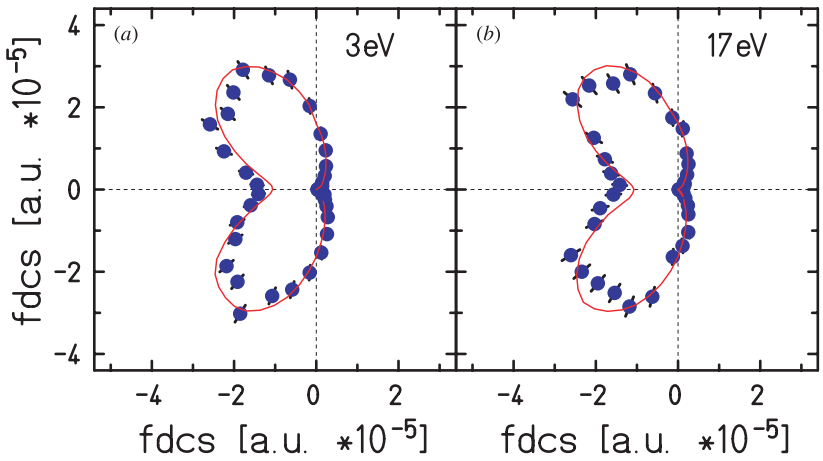

Figure 10. Consistency check for 5DCS from linearly and circularly polarized light following a suggestion of Berakdar [44]. $\theta_A = \theta_B = 90° \pm 10°$. Electron A has no fixed direction in the laboratory frame (see the discussion in section 3). Full circles, sum of 4DCS for LCP and RCP (see text). Full curve, 3C calculation from [32] linearly polarized light, sum of 4DCS for polarization x and y (see equation (1)).

sections for left and right circularly polarized light is identical to the sum over the cross section for linearly polarized light with the polarization tilted by 90° (equation (3)). This interesting result can serve as a consistency check for data obtained with linearly and circularly polarized light. For two energy sharings figure 10 shows this comparison for our data for circularly polarized light and compares it with CCC calculations for linearly polarized light. The latter are in good agreement with experiment [57].

6. Conclusions and open questions

In conclusion we have shown the multidimensional momentum distribution in the two-electron continuum of He ionized by circularly and linearly polarized light. The 4π solid angle was achieved in our experiment for all three particles in the continuum. Circular dichroism is found to be a major effect even for extremely unequal energy sharing. The redundancy in the momentum measurement of our experiment and the data for circular and linearly polarized light taken with the same apparatus at the same beamline allow one to reliably exclude systematic errors. The data taken under much inferior experimental conditions in multi-bunch operation by us reported in [1] have correctly demonstrated the major effect of circular dichroism in the recoil-ion momentum distributions. The transformation to 5DCS, however, must be influenced by a calibration error in our momentum or photon energy calibration. These data are superseded by the present experiment.

We note that even so impressive progress has been made in the theoretical description of the double photo ionization process, still no perfect agreement with the experimental results is achieved for an extremely simple three-body process (see also [33, 55]). Furthermore, none of the theoretical approaches available so far has provided an intuitive physical explanation of what causes the predicted and observed helicity dependence. One step in this direction is given by a parametrization of the 4DCS [56, 58] and by the analysis given in [34, 44]. It shows that circular dichroism is connected to the phase difference between the gerade and ungerade amplitudes contributing to double ionization. Further insight might be gained from an interpretation similar to the circular dichroism observed in one-electron ejection from molecules and non-magnetic solids [52–55, 60]. Here a core level electron is emitted, and the outgoing wave is scattered at the nearest neighbours. For linearly polarized light this scattering leads in many cases to a peak in the electron angular distribution in the direction of this scatterer (forward focusing). If induced by circularly polarized light, this forward peak is observed to rotate in the direction of rotation of the electrical field vector by an angle of m/kR, where m is the magnetic quantum number of the outgoing electron with momentum k and R is the distance to the scatterer. This scattering of a photoelectron at a neighbouring nucleus and photo double ionization are related. Recently, Keller has shown [60] that at the photon energy used in this paper, helium double photoionization is dominated by the TS1 mechanism, i.e. one electron which absorbs the photon knocks out the second electron via e–e scattering. These calculations in many-body perturbation theory confirm the semiempirical finding by Samson [12], who stressed the analogy of double photo ionization and electron impact ionization. It might therefore be possible to construct an analogy between dichroism in photoelectron scattering at neighbouring atoms in a molecule to the dichroism observed in double ionization.

Acknowledgments

This work was supported by DFG, BMBF. RD acknowledges support from the Heisenbergprogramm (DFG). We thank J Berakdar, J Feagin, R D Munio, C Fadley, S Keller, A Kheifets and I Bray for helpful discussions.

References

[1] Mergel V *et al* 1998 *Phys. Rev. Lett.* **80** 5301
[2] Bartlett R J, Walsh P J, He Z X, Chung Y, Lee E-M and Samson J A R 1992 *Phys. Rev.* A **46** 5574

[3] Berrah N, Heiser F, Wehlitz R, Levin J, Whitfield S B, Viefhaus J, Sellin I A and Becker U 1993 *Phys. Rev.* A **48** R1733
[4] Bizau J M and Wuilleumier F J 1995 *J. Electron Spectrosc. Relat. Phenom.* **71** 205
[5] Carlson T A 1967 *Phys. Rev.* **156** 142
[6] Holland D M P, Codling K, West J B and Marr G V 1979 *J. Phys. B: At. Mol. Phys.* **12** 2465
[7] Kossmann H, Schmidt V and Andersen T 1988 *Phys. Rev.* A **60** 1266
[8] Levin J C, Lindle D W, Keller N, Miller R D, Azuma Y, Berrah Mansour N, Berry H G and Sellin I A 1991 *Phys. Rev. Lett.* **67** 968
[9] Levin J C, Sellin I A, Johnson B M, Lindle D W, Miller R D, Berrah N, Azuma Y, Berry H G and Lee D H 1993 *Phys. Rev.* A **47** R16
[10] Levin J C, Armen G B and Sellin I A 1996 *Phys. Rev. Lett.* **76** 1220
[11] Sagurton M, Bartlett R J, Samson J A R, He Z X and Morgan D 1995 *Phys. Rev.* A **52** 2829
[12] Samson J A R 1990 *Phys. Rev. Lett.* **65** 2863
[13] Samson J A R, Bartlett R J and He Z X 1992 *Phys. Rev.* A **46** 7277
[14] Schmidt V, Sandner N, Kuntzemüller H, Dhez P, Wuilleumier F and Källne E 1976 *Phys. Rev.* A **13** 1748
[15] Wehlitz R, Heiser F, Hemmers O, Langer B, Menzel A and Becker U 1991 *Phys. Rev. Lett.* **67** 3764
[16] Wight G R and Van der Wiel M J 1976 *J. Phys. B: At. Mol. Phys.* **9** 1319
[17] Dörner R *et al* 1996 *Phys. Rev. Lett.* **76** 2654
[18] Spielberger L *et al* 1996 *Phys. Rev. Lett.* **76** 4685
[19] Spielberger L *et al* 1995 *Phys. Rev. Lett.* **74** 4615
[20] Dawber G, Hall R I, McConkey A G, MacDonald M A and King G C 1994 *J. Phys. B: At. Mol. Opt. Phys.* **27** L341
[21] Proulx D and Shakeshaft R 1993 *Phys. Rev.* A **48** R875
[22] Briggs J and Schmidt V 2000 *J. Phys. B: At. Mol. Opt. Phys.* **33** R1
[23] Dörner R *et al* 1996 *Phys. Rev. Lett.* **77** 1024
Dörner R *et al* 1997 *Phys. Rev. Lett.* **78** 2031 (erratum)
[24] Bräuning H P *et al* 1997 *J. Phys. B: At. Mol. Opt. Phys.* **30** L649
[25] Pont M and Shakeshaft R 1996 *Phys. Rev.* A **54** 1448
[26] Feagin J M 1996 *J. Phys. B: At. Mol. Opt. Phys.* **29** l551
[27] Dörner R, Mergel V, Jagutzki O, Spielberger L, Ullrich J, Moshammer R and Schmidt-Böcking H 2000 *Phys. Rep.* **330** 96–192
[28] Huetz A and Mazeau J 2000 *Phys. Rev. Lett.* **85** 530
[29] Berakdar J and Klar H 1992 *Phys. Rev. Lett.* **69** 1175
[30] Berakdar J, Klar H, Huetz A and Selles P 1993 *J. Phys. B: At. Mol. Opt. Phys.* **26** 1463
[31] Viefhaus J *et al* 1996 *Phys. Rev. Lett.* **77** 3975
[32] Kheifets A and Bray I 1998 *Phys. Rev. Lett.* **81** 4588
[33] Kheifets A, Bray I, Soejima K, Danjo A, Okuno K and Yagishita A 1999 *J. Phys. B: At. Mol. Opt. Phys.* **32** L501
[34] Berakdar J 1998 *J. Phys. B: At. Mol. Opt. Phys.* **31** 3167
[35] Soejima K, Danjo A, Okuno K and Yagishita A 1999 *Phys. Rev. Lett.* **83** 1546
[36] Schmidt V 1997 *Electron Spectrometry of Atoms using Synchrotron Radiation (Cambridge Monographs on Atomic, Molecular and Chemical Physics vol 6)* (Cambridge: Cambridge University Press)
[37] Ullrich J, Moshammer R, Dörner R, Jagutzki O, Mergel V, Schmidt-Böcking H and Spielberger L 1997 *J. Phys. B: At. Mol. Opt. Phys.* **30** 2917
[38] Dörner R *et al* 1998 *Phys. Rev.* A **57** 1074
[39] Moshammer R, Unverzagt M, Schmitt W, Ullrich J and Schmidt-Böcking H 1996 *Nucl. Instrum. Methods* B **108** 425
[40] Viefhaus J, Avaldi L, Heiser F, Hentges R, Gessner O, Rüdel A, Wiedenhöft M, Wielczek K and Becker U 1996 *J. Phys. B: At. Mol. Opt. Phys.* **29** L729
[41] Achler M 1999 *PhD Thesis* Universität Frankfurt (Berlin: Logos)
[42] Schaphorst S J, Krässig B, Schwarzkopf O, Scherer N, Schmidt V, Lablanquie P, Andric L, Mazeau L and Huetz A 1995 *J. Electron Spectrosc. Relat. Phenom.* **76** 229
[43] Kimura H, Miyahara T, Gota J, Mayama K, Yanagihara M and Yamamoto M 1995 *Rev. Sci. Instrum.* **52** 1920
[44] Berakdar J 1999 *J. Phys. B: At. Mol. Opt. Phys.* **32** L25
[45] Maulbetsch F and Briggs J S 1995 *J. Phys. B: At. Mol. Opt. Phys.* **28** 551
[46] Schwarzkopf O, Krässig B, Elmiger J and Schmidt V 1993 *Phys. Rev. Lett.* **70** 3008
[47] Schwarzkopf O, Krässig B, Schmidt V, Maulbetsch F and Briggs J 1994 *J. Phys. B: At. Mol. Opt. Phys.* **27** L347–50
[48] Lablanquie P, Mazeau J, Andric L, Selles P and Huetz A 1995 *Phys. Rev. Lett.* **74** 2192

[49] Huetz A, Selles P, Waymel D and Mazeau J 1991 *J. Phys. B: At. Mol. Opt. Phys.* **24** 1917
[50] Feagin J and Berakdar J Private communication
[51] Daimon H, Ynzunza R X, Palomares F J, Tober E D, Wang Z X, Kaduwela A P, Van Hove M A and Fadley C S 1998 *Phys. Rev.* B **58** 9662
[52] Daimon H, Nakatami T, Imada S, Suga S, Kagoshima Y and Miyahara T 1993 *Japan. J. Appl. Phys.* 2 **32** L1480
[53] Kaduwela A P, Xiao H, Thevuthasa S, Fadley C S and Van Hove M A 1995 *Phys. Rev.* B **52** 14927
[54] Ynzunza R X *et al* 2000 *J. Electron Spectrosc. Relat. Phenom.* **106** 7
[55] Cvejanovic S, Wightman J P, Reddish T J, Maulbetsch F, MacDonald M A, Kheifets A S and Bray I 2000 *J. Phys. B: At. Mol. Opt. Phys.* **33** 265
[56] Malegat L, Selles P and Huetz A 1997 *J. Phys. B: At. Mol. Opt. Phys.* **30** 251
[57] Bräuning H P *et al* 1998 *J. Phys. B: At. Mol. Opt. Phys.* **31** 5149
[58] Malegat L, Selles P, Lablanquie P, Mazeau J and Huetz A 1997 *J. Phys. B: At. Mol. Opt. Phys.* **30** 263
[59] Van Hove M A, Kaduwela A P, Xiao H, Schattke W and Fadley C S 1996 *J. Electron Spectrosc. Relat. Phenom.* **80** 137
[60] Keller S 2000 *J. Phys. B: At. Mol. Opt. Phys.* **33** L513